Scaling of nonaffine deformation in random semiflexible fiber networks

H. Hatami-Marbini and R. C. Picu
Department of Mechanical, Aerospace and Nuclear Engineering, Rensselaer Polytechnic Institute, Troy, New York 12180, USA
(Received 11 January 2008; revised manuscript received 12 April 2008; published 19 June 2008)

Random networks of semiflexible filaments play a crucial role in the mechanics of many systems, including the cell. To understand the response of semiflexible networks to stress, a strain-based measure of nonaffine deformation is introduced and used to probe the mechanics on various scales. This measure provides a unified description of nonaffinity in both strain and rotation and indicates that the level of nonaffinity in these quantities in a given system is comparable. The degree of nonaffinity decreases as the scale of observation increases. This scaling is a power law with different exponents for length scales smaller and larger than a characteristic length scale proportional to the fiber length. The fiber bending stiffness controls the scaling at small length scales, while the large length scale scaling exponent is independent of fiber density and stiffness.

DOI: 10.1103/PhysRevE.77.062103 PACS number(s): 46.65.+g, 42.81.Uv, 64.60.aq

The study of semiflexible polymer networks is essential in understanding the mechanical properties of many polymeric and biological materials. Examples of fiber networks are the cytoskeleton of eukaryotic cells and other biological networks [1–3], paper [4], battery substrates [5], and tissue templates [6]. The fibers may be densely or sparsely cross-linked and the elastic strain energy is due to both stretching and bending deformation of the fibers. The relationship between the overall behavior of the network and the fiber properties and distribution (the "microstructure") is complex and still a matter of debate, in particular for semiflexible networks. This issue has been discussed in the literature primarily in connection with the mechanics of the cell, which is controlled by that of the cytoskeleton—a random fiber network of filamentous proteins.

The deformation of random, cross-linked fiber networks is nonaffine [7–9] i.e., the strain measured locally is different from the applied far field strain. Nonaffine deformation has been evidenced in other disordered systems, such as granular materials and glasses [10–12], in polymeric and biological materials (e.g., [13]). In fiber networks, nonaffine deformation leads to the decrease of the effective elastic moduli relative to those expected based on the affine assumption [8,9,13]. In granular packing, nonaffine motion of the grains leads to enhanced dissipation and an abnormally high loss modulus [14]. It appears that in order to identify the microscopic origins of the system scale mechanical properties of such materials, proper understanding of the nonaffine deformation is required [15].

Various measures of nonaffinity have been used. Langer and Liu [16] studied the response of foams to small perturbations using three measures of nonaffinity, two of which are based on bubble displacements ($\delta\mathbf{u}=\mathbf{u}-\mathbf{u}^{\mathrm{aff}}$, where $\mathbf{u}$ is the actual displacement of a bubble and $\mathbf{u}^{\mathrm{aff}}$ is the corresponding affine displacement) and one is based on energies. The same nonaffine displacement, $\delta\mathbf{u}$, was used by Tanguy *et al.* [11,12] who studied the deformation of amorphous bodies made from polydisperse Lennard-Jones beads. These are vectorial quantities computed at the site of each discrete entity of the ensemble. Head *et al.* [7] studied nonaffinity in networks of semiflexible polymers subjected to shear and used a scalar measure based on the infinitesimal change of the angle θ made by a vector connecting two nodes in the structure with one of the global axes, $\delta\theta^2(r)=\langle(\theta-\theta^{\mathrm{aff}})^2\rangle_r$. This quantity is evaluated as an ensemble average over vectors of a given length, r. Onck *et al.* [9] showed that the degree of nonaffinity decreases as the network is subjected to large deformations and employed a scalar measure equivalent to the average of the ratio $\|\delta\mathbf{u}/\mathbf{u}^{\mathrm{aff}}\|$. A detailed study of the scaling behavior of nonaffinity correlation functions of the form $\langle\delta u_i(x)\delta u_j(0)\rangle$ was performed by DiDonna and Lubensky [17].

The characteristic lengths playing a role in the mechanics of fiber networks are the fiber length, L_0, the mean segment length, l_c (or the fiber number density, N) and a parameter with units of length which represents the relative importance of the bending, κ, and stretching, η, moduli, $l_b=\sqrt{\kappa/\eta}$. The system size (a square domain of dimension L) is an additional length scale. These four parameters are independent and one may be chosen for normalization. Here we normalized all lengths by L_0.

It has been discussed that in the high density limit (large N or small l_c), the shear modulus scales linearly with the fiber density approaching the affine prediction [8]. A similar trend is observed upon increasing the bending stiffness κ (large l_b) [7]. In the other limit, when the bending rigidity and/or the fiber number density are low, the nonaffinity is important and the shear modulus is smaller than predictions obtained based on the affine approximation. Head *et al.* [7] define a scalar function of these material length scales, λ, which can be used to determine whether a given network deforms affinely or not at small strains.

In this Brief Report we introduce a strain-based nonaffinity measure and study the effects of N (or l_c/L_0) and of l_b/L_0 on the nonaffine deformation of random networks. We observe power-law variation of nonaffinity with the probing length scale for a broad range of scales; we conclude that all networks deform nonaffinely, even at large N, and discuss the essential role the fiber length L_0 plays in this scaling.

The systems considered here are two-dimensional (2D) random fiber networks obtained by randomly placing fibers of length L_0, having random orientation, in a square domain of linear dimension L. $L_0=0.5$ for all results reported below, except where stated otherwise. This length scale is used for normalization. Rigid connections are defined at all points

where fibers cross. The dangling ends do not contribute to the energetics of the system (since excluded volume effects are not considered). Each fiber has bending stiffness κ and axial stiffness η. The system acquires overall rigidity at a critical point defined by a critical fiber density [8]. The system is loaded by displacement-imposed boundary conditions (small strains). Uniaxial, biaxial, and shear loading are considered. The solution is obtained via energy minimization (performed using a finite element solver), where the total energy is computed as the sum of strain energies associated with bending and axial deformation of fibers over the entire system.

Once the nodal displacements are obtained, strains can be computed on various probing length scales. This is performed using the method commonly employed in tensometry. In this technique, strain gages are applied on the surface of a deforming body and the normal strain in the direction of the gage is measured by the variation of the length and/or electrical resistivity of the respective wire. Measurement of normal strains in three different directions is sufficient to determine the entire strain tensor (plane strain). It is important to note that each gage provides the mean strain, $\frac{1}{l}\int_0^l \varepsilon_{ij}(x)dx$, over its span, l. Here we probe the computed field by selecting triplets of nodes defining triangles with shape close to equilateral and evaluate the strain based on the displacements of this set of nodes. If the length of each edge of a given triangle is l, the resulting strain tensor is considered to be an average of the underlying field over the length scale $r=\sqrt{A}=(3^{1/4}/2)l$, where A is the area of the respective triangle. Note that the compatibility condition is fulfilled since we first compute the displacements. The corresponding affine strain components, $\varepsilon_{ij}^{\text{aff}}$, are the far field and obviously $\langle \varepsilon_{ij} \rangle_r = \varepsilon_{ij}^{\text{aff}}$ for all length scales r.

The measure of nonaffinity used here is defined by the fluctuation of the actual deformation gradients relative to their affine estimate,

$$\mathbf{H}(r) = \langle (\Xi - \Xi^{\text{aff}})^2 \rangle_r, \tag{1}$$

where $\Xi=(\varepsilon_{11}\ \varepsilon_{22}\ \varepsilon_{12}\ \omega_{12})$ and ε_{ij} and ω_{12} are strain and rotation components, respectively. The index r denotes the length scale on which $\mathbf{H}$ is evaluated. We note that $\mathbf{H}$ does not possess tensorial properties.

As opposed to other measures used in the literature, $\mathbf{H}$ naturally separates the strain and the rotation components of the displacement gradient field. It also provides an average over scales finer than r. It is independent of the far field loading. Furthermore, it is better suited for direct comparison with continuum models, in the appropriate limit, than other measures in the literature.

The results presented below are obtained considering fiber number densities N ranging from 80 to 800 fibers per unit area (all corresponding to systems above the rigidity percolation threshold) and square models of linear dimensions $L=1$ and 10 ($L/L_0=2$ and 20). The ratio l_b is varied from 5×10^{-3} to 5×10^{-6} (l_b/L_0 from 10^{-2} to 10^{-5}) representing fibers with large and small bending stiffness.

Figure 1 shows the four nonzero components of the nonaffinity measure of Eq. (1) versus the probing length scale r. The far field loading is uniaxial extension in the x_1 direction.

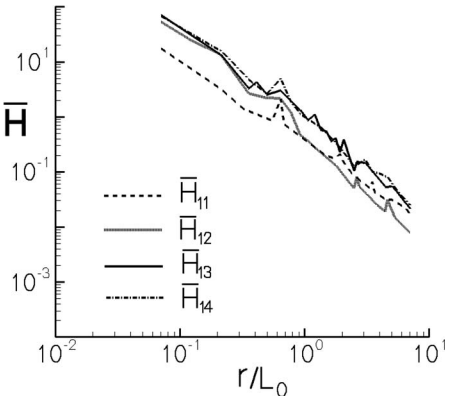

FIG. 1. Components of the normalized nonaffinity measure tensor $\overline{\mathbf{H}}(r)=\mathbf{H}(r)/\varepsilon_0^2$ against the normalized probing length scale, r/L_0, for a network of density $N=150$ fibers per unit area, $l_c/L_0=0.046$, and $l_b=5\times10^{-5}$ ($l_b/L_0=10^{-4}$). The normalization of the vertical axis is performed with the applied "far field" uniaxial strain ε_0.

Here and in the following figures, the vertical axis is normalized by the square of the applied far field strain, $\varepsilon_{11}^{\text{aff2}}=\varepsilon_0^2$. It is observed that all strains exhibit nonaffine fluctuations of comparable magnitude. Moreover, the nonaffinity in the rotation ω_{12} is similar to that of the strains. This relates to multiple observations of "rotatory structures" in the nonaffine displacements of granular materials [12]. This is the first important result of this work: $\mathbf{H}$ represents both strain and rotation in a unified way allowing for a quantitative comparison of the rotation and strain nonaffinity.

All nonaffinity measures follow a power-law scaling with r over the entire range of probed length scales. Similar conclusions are obtained for other far field loadings, for the rotation component of $\mathbf{H}$ and the strain component associated with the imposed far field.

This type of result is reported by Head *et al.* [7] for fiber networks and using their measure of nonaffinity, within a certain range of l_b/L_0. Tanguy *et al.* [11] suggest that in granular systems the nonaffinity decays to zero at a distance of about 30 times the grain size from the point where the perturbation is applied. The present data suggest that nonaffinity is always nonzero, albeit small, at large length scales. However, the system has no characteristic length scale that separates the affine from the nonaffine mechanical response. This conclusion is obtained here for relatively sparse networks with $l_c/L_0=0.046$ and flexible fibers with $l_b/L_0=10^{-4}$, but holds true for all other systems investigated, as discussed below.

Figure 2 shows the effect of the fiber number density, N, on $\mathbf{H}(r)$. N is varied from 80 to 800 fibers per unit area (l_c/L_0 from 0.009 to 0.079, or L_0/λ from 6.30 to 113.52) and $l_b=5\times10^{-3}$ ($l_b/L_0=10^{-2}$). These fibers are much stiffer in bending than those used to produce the data in Fig. 1. Only the nonaffinity in the normal strain component in direction x_1 due to far field uniaxial extension in the same direction is shown. The other nonaffine strain components behave similarly (Fig. 1).

A few interesting conclusions emerge. The nonaffinity is more pronounced in systems of low density, which is in

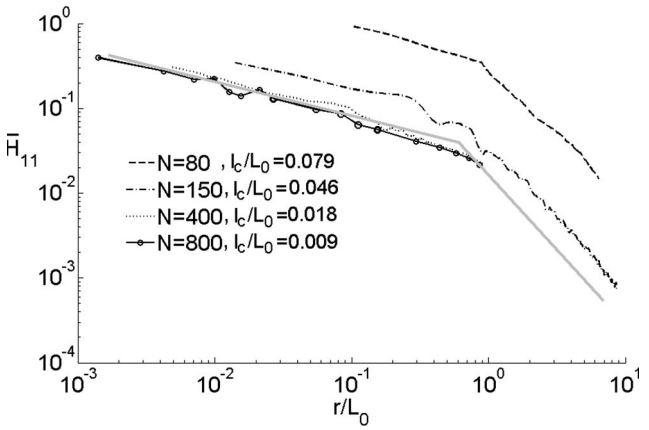

FIG. 2. Component $\bar{H}_{11}=H_{11}/\varepsilon_0^2$ of the normalized nonaffinity measure versus the normalized probing length scale, r/L_0, for systems of various fiber number density and $l_b=5\times10^{-3}(l_b/L_0=10^{-2})$. The gray continuous line is added to emphasize the two distinct scaling regimes discussed in the text.

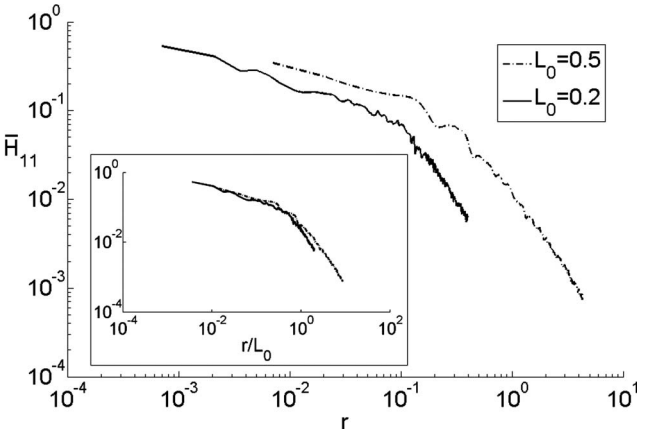

FIG. 3. Component $\bar{H}_{11}=H_{11}/\varepsilon_0^2$ of the normalized nonaffinity measure versus the probing length scale, r, for two systems with fiber length $L_0=0.2$ and 0.5 subjected to uniaxial strain ε_0. The inset shows the same data after normalization of the horizontal axis by the respective fiber length. The scaling crossover depends on l_b (Fig. 4), but is independent of N (Fig. 2).

agreement with previous observations [7,8]. The data follow two well-defined power-law scaling regimes, with a smaller scaling exponent of 0.42 ± 0.03 for $r/L_0<r^*/L_0$ and a larger one of 1.65 ± 0.05 at large probing length scales. We will return to the physical significance of the characteristic length scale r^*/L_0. This behavior and r^*/L_0 are independent of N which has exclusively the effect of shifting the curves in the vertical direction. This is the second important result of this work. The data for the densest two systems were obtained with a simulation cell of dimension $L=1$, which does not influence the scaling, but prevents obtaining the second scaling regime at large r/L_0. The continuous gray line is added to emphasize the two regimes.

It is observed that at densities above a certain threshold (between $N=200$ and 400, $l_c/L_0=0.035$ and 0.018, respectively), the nonaffinity becomes insensitive to the fiber density but does not vanish. In this regime the overall moduli of the network asymptote to the affine values [7] (the curves for $N=400$ and 800 correspond to the parameter L_0/λ in [7] having values 46.45 and 113.52, respectively). Since the nonaffinity is not exactly zero on any probed length scale, computing the moduli using the affine assumption can only be an approximation. Strictly speaking, for a given (finite) model size there is no convergence to an affine homogeneous continuum for denser networks.

To clarify the origin of the characteristic scale r^*/L_0 we consider systems of the same density and fiber stiffness, but with different fiber length, L_0. Figure 3 shows data similar to those in Fig. 2 for systems with $N=150$, $l_b=5\times10^{-3}$ and with $L_0=0.2$ and 0.5. The horizontal axis of the main figure is not normalized. The inset shows the same data after normalization of the abscissa by the respective fiber length. It is seen that the change in scaling behavior at length scales below and above r^*/L_0 is related to the fiber length and $r^*/L_0\approx0.5$. This indicates that the structure of the network controlling the nonaffine mechanical response is different when probed at length scales below and well above the fiber length. This issue will be discussed further in a forthcoming presentation. Further support for the role played by L_0 in this discussion comes from the data in the next figure. It is also interesting to observe that the scaling exponents are independent of L_0.

Let us turn now to the effect of the fiber bending stiffness, parameter l_b, on the nonaffine deformation. Figure 4 shows the first component of the nonaffinity measure (1) for systems with $N=150$ and $L_0=0.5$ ($l_c/L_0=0.046$), and various l_b's ($l_b/L_0=10^{-2}$ to 10^{-5}). The curve corresponding to the largest value of l_b considered is reproduced from Fig. 2. It is observed that reducing the fiber bending stiffness (relative to its axial stiffness) leads to more pronounced nonaffinity on all scales (curves shift up). This was reported in previous studies (e.g., [7]). As l_b decreases, the scaling exponent at large r/L_0 does not change; however, the slope of the curve at small r/L_0 increases. In the limit of very flexible fibers, the scaling is characterized by a single exponent: That measured at large r/L_0 in all systems studied.

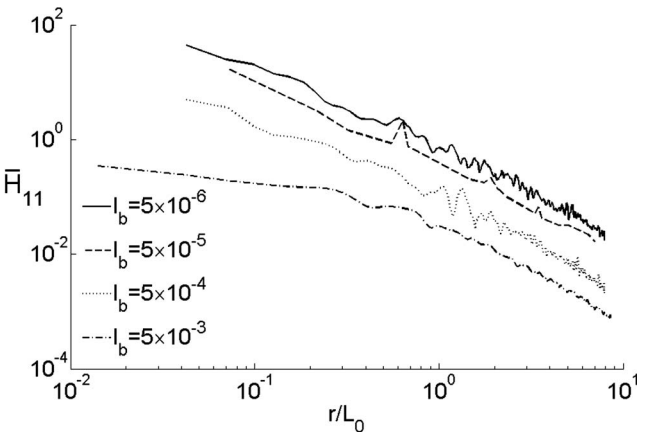

FIG. 4. Normalized nonaffinity measure ($\bar{H}_{11}=H_{11}/\varepsilon_0^2$) against the normalized probing length scale, r/L_0, for networks with different l_b's and same number of fibers per unit area, $N=150$ ($l_c/L_0=0.046$). Two distinct slopes are observed for the system with larger l_b, while as l_b decreases, the scaling observed at large r/L_0 becomes dominant.

The observation that decreasing l_b eliminates the scaling regime at low r/L_0 provides support to the discussion above regarding the role of the fiber length. As l_b decreases, fiber segments between neighboring cross-links behave more like trusses. Therefore, the contiguity of fibers becomes less important and L_0 loses it mechanical relevance.

The data in Fig. 4 can be compared with the results of Head *et al.* [7]. Their nonaffinity measure, $\delta\theta^2(r)=\langle(\theta-\theta^{\text{aff}})^2\rangle_r$, exhibits the behavior shown here for $\mathbf{H}(r)$ when l_b is small (power-law scaling with r with a single exponent). At large l_b (or L_0/λ in the notation of [7]), $\mathbf{H}(r)$ exhibits scaling described by two exponents (Figs. 3 and 4), while $\delta\theta^2(r)$ appears to reach a plateau at small r/L_0. This saturation of $\delta\theta^2(r)$ was used as an argument to approximately divide the networks "affine" and "nonaffine", based on parameter L_0/λ (which is proportional to l_b). Our data do not exhibit this saturation trend and therefore do not support this dichotomy. The absence of a plateau is clearly seen in both Figs. 1 and 4. Support for this view is provided by the experimental data in [18]. In this reference, the authors measured the nonaffinity of the deformation field of networks of semiflexible polymers and obtained a power-law scaling over the entire probed range of scales. Their data correspond to the small scaling exponent regime in Fig. 2.

The systems considered in Fig. 4 span the transition of the overall shear modulus G of the network discussed in [7,8] from a regime in which $G\propto\kappa$, at small l_b/L_0, to a regime in which $G\sim G_{\text{affine}}\propto\eta$, at large l_b/L_0. For the four systems with l_b/L_0 equal to 10^{-5}, 10^{-4}, 10^{-3}, and 10^{-2}, L_0/λ is equal to 2.79, 6.01, 12.95, and 27.89, respectively. As discussed in connection with Fig. 2, none of these systems deform affinely. However, when one sets the length scale of observation (probing the overall network moduli sets $r/L_0=L/L_0$; also note that $L>L_0$ and hence $L/L_0>r^*/L_0$, i.e., probing on the "system scale" is performed in the scaling range characterized by the large slope), the nonaffinity decreases upon increasing l_b/L_0. Further increasing l_b/L_0 leads to a smaller shift of the curves in Fig. 4 toward lower values, which is in agreement with the overall shear modulus G approaching the affine value G_{affine} in this range of l_b/L_0.

In conclusion, the mechanics of random fiber networks is controlled by nonaffine deformation on all scales; the nonaffinity scales as a power law with the scale of observation. Two scaling regimes are observed: One with a small exponent at length scales smaller than the fiber length and a second one characterized by a larger exponent at larger length scales. Decreasing the fiber bending stiffness leads to the reduction of the distinction between these two regimes.

[1] P. A. Janmey, Curr. Opin. Cell Biol. **3**, 4 (1991).
[2] A. R. Bausch and K. Kroy, Nat. Phys. **2**, 231 (2006).
[3] C. Storm, J. J. Pastore, F. C. Mackintosh, T. C. Lubensky, and P. A. Janmey, Nature (London) **435**, 191 (2005).
[4] M. Alava and K. Niskanen, Rep. Prog. Phys. **69**, 669 (2006).
[5] C. W. Wang, X. Cheng, A. M. Sastry, and S. B. Choi, J. Eng. Mater. Technol. **121**, 503 (1999).
[6] P. L. Chandran and V. H. Barocas, J. Biomech. Eng. **128**, 259 (2006).
[7] D. A. Head, A. J. Levine, and F. C. MacKintosh, Phys. Rev. E **68**, 061907 (2003).
[8] J. Wilhelm and E. Frey, Phys. Rev. Lett. **91**, 108103 (2003).
[9] P. R. Onck, T. Koeman, T. van Dillen, and E. van der Giessen, Phys. Rev. Lett. **95**, 178102 (2005).
[10] H. M. Jaeger, S. R. Nagel, and R. P. Behringer, Rev. Mod. Phys. **68**, 1259 (1996).
[11] A. Tanguy, J. P. Wittmer, F. Leonforte, and J. L. Barrat, Phys. Rev. B **66**, 174205 (2002).
[12] F. Leonforte, A. Tanguy, J. P. Wittmer, and J. L. Barrat, Phys. Rev. B **70**, 014203 (2004).
[13] F. C. MacKintosh, J. Kas, and P. A. Janmey, Phys. Rev. Lett. **75**, 4425 (1995).
[14] A. J. Liu, S. Ramaswamy, T. G. Mason, H. Gang, and D. A. Weitz, Phys. Rev. Lett. **76**, 3017 (1996).
[15] C. Heussinger and E. Frey, Phys. Rev. Lett. **96**, 017802 (2006).
[16] S. A. Langer and A. J. Liu, J. Phys. Chem. B **101**, 8667 (1997).
[17] B. A. DiDonna and T. C. Lubensky, Phys. Rev. E **72**, 066619 (2005).
[18] J. Liu, G. H. Koenderink, K. E. Kasza, F. C. MacKintosh, and D. A. Weitz, Phys. Rev. Lett. **98**, 198304 (2007).